2005-10-19

Detection of early antiangiogenic effects in human colon adenocarcinoma xenografts: in vivo changes of tumor blood volume in response to experimental VEGFR tyrosine kinase inhibitor

Young Ro Kim

Et al.

Detection of Early Antiangiogenic Effects in Human Colon Adenocarcinoma Xenografts: *In vivo* Changes of Tumor Blood Volume in Response to Experimental VEGFR Tyrosine Kinase Inhibitor

Young Ro Kim, Anna Yudina, JoseLuis Figueiredo, Wilfried Reichardt, Dana Hu-Lowe, Alexander Petrovsky, Hye Won Kang, Denise Torres, Umar Mahmood, Ralph Weissleder, and Alexei A. Bogdanov, Jr.

Center for Molecular Imaging Research, Massachusetts General Hospital, Charlestown, Massachusetts

Abstract

Antiangiogenesis is emerging as efficient strategy for targeting and potentially eliminating neoplastic tumor vessels. The main goal of this study was to establish whether absolute tumor blood volume (V_b) change could be used as an early predictor of antiangiogenesis in ectopic and orthotopic colon carcinomas. To assess therapy-induced changes of V_b, we did comparative analysis of signal intensities in tumors and muscle using steady-state magnetic resonance imaging (MRI) assisted with an intravascular paramagnetic contrast agent [gadolinium-labeled protected graft copolymer (PGC-Gd)]. Athymic mice with implanted human MV522 tumors were treated with vascular endothelial growth factor type 2 receptor tyrosine kinase inhibitor (VEGFR2-TKI) that has been shown to inhibit VEGFR2 phosphorylation and tumor growth *in vivo*. Animals were imaged either after a single day or after a 1-week course of treatments. The measured V_b in ectopic tumors was 2.5 $\pm$ 1.5% of total tissue volume 1 week after the implantation (n = 8). Two doses of VEGFR2-TKI (25 mg/kg, p.o., b.i.d.) resulted in a decrease of V_b to 1.3 $\pm$ 0.3%. In orthotopic tumors, the measured V_b was initially higher (11.9 $\pm$ 2.0%); however, VEGFR2-TKI treatment also resulted in a statistically significant decrease of V_b. The absolute V_b was not affected in the muscle as a result of treatments. MRI measurements were corroborated by using isotope and correlative histology experiments. Our results show that steady-state MRI is highly sensitive to early antiangiogenic effects caused by small molecule drugs. (Cancer Res 2005; 65(20): 9253-60)

Introduction

Vascular endothelial growth factor (VEGF) type 2 receptor (VEGFR2, Flk-1/KDR) is one of the major regulators of vasculogenesis and angiogenesis. The detailed analysis of the role of VEGFR2-mediated signal transduction suggested that the inhibition of VEGFR pathway would provide a powerful antiangiogenic signal that could be highly useful in inhibiting pathogenic angiogenesis (e.g., in cancer progression). The first anti-VEGF targeted drug (bevacuzimab, Genentech, Inc., San Francisco, CA) has already been approved in combination with the first-line chemotherapy for treating metastatic colorectal cancer (reviewed in ref. 1).

To date, several small molecule VEGFR2 kinase (KDR) inhibitors have been tested in animal cancer models and resultant changes in tumor vasculature have been described. Strong antiangiogenic responses induced by SU5416 and SU6668 were previously shown (2, 3). Decrease in tumor vascular density and vessel diameter and higher blood flow in remnant tumor vessels were typical drug-induced effects observed in animal models of cancer. Strong antimetastatic and antiproliferative responses resulting in tumor and endothelial cell apoptosis were reported (4). Similar findings of reduced microvascular density, blood flow changes, as well as inhibition of VEGF-mediated vascular permeability have been reported after treating animals with SU11248 (5), PTK787/ZK 222584 (6, 7), CGP 41251 (8), and protein kinase C (PKC) 412 (9). Some of the above inhibitors had variable selectivities and at least partially blocked platelet-derived growth factor (PDGF)-β– and PKC-mediated signal transduction. Recently, an experimental VEGFR inhibitor, AG013736 (Pfizer, La Jolla, CA), showed efficient endothelial cell regression with a 70% decrease of vascular density in experimental tumors (10).

Noninvasive *in vivo* magnetic resonance imaging (MRI) of antiangiogenic effects (11, 12) was instrumental in many of the above studies (reviewed in refs. 13–16). The principal advantages of noninvasive MRI are that (*a*) high anatomic resolution images could be acquired repeatedly; (*b*) no ionizing radiation could affect therapy assessment in preclinical studies; (*c*) the measurements are done throughout the total tumor volume and provide global rather than regional data; and (*d*) the results of antiangiogenic treatments could be potentially detected at the early phase of the treatment. The changes in tumor blood volume and flow detectable with MRI in many cases precede gross morphology changes that result from long-term effects of antiangiogenic treatment.

The changes in tumor blood volume can be assessed by several fundamentally different MRI techniques. Intravascular T1 agents (i.e., predominantly affecting longitudinal relaxation of proton magnetization; ref. 17) enable quantifying the absolute blood volume fraction (18). The probes affecting T2 relaxation [i.e., agents affecting spin-spin relaxation of water proton magnetization, e.g., a bolus of paramagnetic chelate (19) or superparamagnetic nanoparticles (20)], allow V_b measurements by

Note: A.A. Bogdanov, Jr. is currently at Department of Radiology, University of Massachusetts Medical School, Worcester, MA 01655; Y.R. Kim is currently at Athinoula A. Martinos Center for Biomedical Imaging Department of Radiology, Massachusetts General Hospital, Boston, Massachusetts; and D. Hu-Lowe is currently at Pfizer Global Research and Development, San Diego, California.

Requests for reprints: Alexei A. Bogdanov, Jr., Department of Radiology, University of Massachusetts Medical School, 55 Lake Avenue North, Worcester, MA 01655. Phone: 508-856-5571; Fax: 508-856-1860; E-mail: Alexei.Bogdanov@umassmed.edu.

doi:10.1158/0008-5472.CAN-03-2619

the dephased proton population (21). In general, signal intensity enhancement created by intravascular T1 agents is usually regarded as being affected by blood volume and intravascular-extravascular water exchange. On the other hand, the signal intensity reduction caused by a T2 contrast agent depends on blood volume and geometry of vasculature (i.e., vessel radius; ref. 22). When compared with the T2 technique, the method using T1 relaxation provides means to calculate the absolute blood volume independently of geometric factors if a strictly intravascular paramagnetic probe is used under valid water proton exchange conditions (23). In addition, spectroscopic imaging of tumor blood volume utilizing fluorine-19 nuclear MRI was also found feasible (24).

The goal of this study was to determine whether inhibition of VEGFR2-mediated signaling results in early changes of tumor blood volume that could be measured with high precision using a steady-state contrast-enhanced MRI (23, 25). Therefore, we set forth to evaluate early response to the experimental VEGFR2 kinase indazole inhibitor AG013925 (Pfizer) in MV522 human colon carcinoma-bearing mice. A radionuclide-based method was then used to correct blood volume data, followed by a histologic characterization of tumors to determine the influence of antiangiogenesis on cell survival. Antiangiogenic effects were initially investigated in s.c. (ectopic) MV522 tumor models, followed by the verification of treatment effects in a high-resolution study of orthotopic tumors implanted in the colon.

Materials and Methods

Cell culture. Human MV522 colon carcinoma cells were supplied by Pfizer Global Research and Development (La Jolla, CA) and propagated in 10% fetal bovine serum, RPMI (Cellgro, Mediatech, Washington, DC). Red fluorescent MV522 cell line stably expressing DsRed2 (MV522-DsRed2) was obtained as described in ref. 26.

Imaging agent. Protected graft copolymer bearing covalently linked gadolinium-diethylenetriaminepentaacetic acid residues (PGC-Gd) was synthesized and purified as described before (27, 28). The batches of PGC-Gd were characterized on size-exclusion high-performance liquid chromatography column (TSK3000SW, Supelco, Bellefonte, PA) and gadolinium concentrations were determined by the elemental analysis. The polymer was dissolved at 50 mg/mL (13 mmol/L Gd) in Dulbecco's PBS (pH 7) and sterile filtered.

Fluorescent probes. Anti-digoxigenin F(ab′)$_2$ fragment (Roche Diagnostics, Indianapolis, IN) was labeled with Cy3-monohydroxysuccincimide ester (Amersham Biosciences, Piscattaway, NJ; ref. 26). Tomato (*L. esculentum*) lectin was labeled using Alexa Fluor 488-hydroxysuccinimide ester (Molecular Probes Inc., Eugene, OR). Fluorescent conjugates were purified using Bio-Spin P-30 columns (Bio-Rad, Hercules, CA).

Tumor models. The procedures below were approved by the Massachusetts General Hospital Animal Care and Use Committee. Colon carcinoma xenografts were grown ectopically in athymic mice (*nu/nu*, 6 to 8 weeks old, 20 to 25 g, Massachusetts General Hospital Radiation Oncology breeding facilities) as described in refs. 29, 30. Briefly, MV522 cells were harvested 1 day after reaching monolayer density. Two million cells in 100 μL of serum-free cell culture medium were injected s.c. in lower flanks of the mice. Seven days after the implantation of cells, animals with tumors of an average size of ~4 mm in diameter were divided into two groups (treatment and control). Control animals received 0.5% carboxymethylcellulose (CMC) placebo (group 1, n = 3), whereas treated animals received two doses of 25 mg/kg AG013925 homogenized in 0.5% CMC p.o. b.i.d. (group 2, n = 3, delay between doses: 12 hours). Tumor volumes were determined using caliper method. Additional groups of animals underwent a long-term treatment with the inhibitor for 6 to 8 days (12-16 treatments; group 4, n = 3) and compared with a control group, which received placebo only for 6 to 8 days (group 3, n = 3). A total of three independent experiments were done (total n = 36 mice). On the completion of treatment schedule, the animals were subjected to MRI (see below).

For orthotopic implantation, the peritoneal cavity was surgically exposed, the descendent colon was isolated, and 2×10^6 MV522-DsRed2 cells suspended in 20 μL HBSS were injected into the colon wall under direct visualization with the aid of a dissecting microscope. Three weeks postimplantation, colon tumor growth was verified by fluorescence colonoscopy as described in ref. 31. After the tumor was localized using visible and fluorescent light, animals were divided into two groups (n = 4, each group) and treated with VEGFR2-TKI or placebo as described above. The treatment was followed by a high-resolution MRI on 9.4T Bruker instrument (see below).

Magnetic resonance imaging of mice and data analysis. Mice were anesthetized using an i.p. injection of ketamine (80 mg/kg) and xylazine (9 mg/kg) and placed on top of a plastic flask filled with warm water to reduce imaging artifacts and to maintain normal mouse body temperature. Custom-made 30-G catheters were inserted into the tail vein and attached to a microheparin/saline flush. Anesthetized mice were placed prone with tumors located at the center of a 3-in. surface coil and covered with thermoinsulating sheet to prevent hypothermia. MRI data were collected using a 1.5-T Signa scanner (General Electric Medical Systems, Milwaukee, WI) and a three-dimensional spoiled gradient recalled (SPGR) pulse sequence. First, a pre-contrast image was obtained followed by a post-contrast image after the i.v. injection of PGC-Gd (50 μmol Gd/kg in 0.1 mL saline). For V_b measurements, magnetic resonance images (matrix = 256 × 256; 28 transverse slices, slice thickness = 0.7 mm) were collected with TR/TE = 30/4.1 ms and flip angles = 40°, 60°, and 80° and field of view of 10 cm. The entire MRI protocol required 45 minutes. Measurement errors due to blood inflow at both edges of imaging slab were avoided by collecting the data only at the central slices. The pre- and post-contrast agent MRI signal intensities in the blood were measured in large vessels (~40-60 voxels were measured across the central slices). Region-of-interest selection and the analysis of time course of magnetic resonance signal data were made using AFNI shareware package (32). Longitudinal relaxation time (T1) in the blood was calculated by fitting the experimental blood signal intensity dependence of three-dimensional fast SPGR pulse sequence parameters using Matlab software (The Mathworks, Inc., Natick, MA). Imaging of mice with orthotopic colon tumors was done as above except that 9.4T Bruker system was used and the matrix and slice thickness were 256 × 256 and 0.5 mm with TR/TE = 40/5.5 ms, respectively. Additional spin-echo images were acquired with matrix = 512 × 512, slice thickness = 0.5 mm, and TR/TE = 3,000/30 ms. Animals were maintained at 37°C under isoflurane anesthesia.

Tissue blood volume (V_b) was calculated as follows:

$$V_b = (SI_{post\_tissue} - SI_{pre\_tissue})/(SI_{post\_blood} - SI_{pre\_blood}) \quad (1)$$

where SI_{post_tissue} and SI_{post_blood} indicate signal intensities measured in tissue or the blood, respectively, after the administration of contrast agent (PGC-Gd); SI_{pre_tissue} and SI_{pre_blood} indicate signal intensities measured in tissue or the blood, respectively, before the administration of the above contrast agent.

The calculation of V_b using this formula was valid assuming (a) near-constant concentration of PGC-Gd in the blood during the first 45 minutes after the i.v. administration (25, 27); (b) the complete exclusion of PGC from RBC; (c) fast exchange of water across the RBC plasma membrane; and (d) slow water exchange across endothelial barrier. The effects of water exchange rate on blood volume depend on MRI pulse sequence parameters. Therefore, the measured dependence of blood volume on pulse sequence parameters was used to assess water exchange rates across the vascular barrier as described previously (23, 33).

Radioisotope study. RBC content of tumoral and muscle blood supplies was accounted for in an isotope study using RBC labeled using UltraTag kit (Mallinckrodt Medical, St. Louis, MO) designed for *ex vivo* labeling of erythrocytes with ^{99m}Tc pertechnetate. RBCs were isolated from 1 to 1.5 mL of blood obtained from a syngeneic mouse. The total blood was then used

for labeling according to the instructions provided by the manufacturer (1 mCi ^{99m}Tc/labeling reaction). The ^{99m}Tc-labeled RBCs were purified using Hypaque-1077 (Sigma Chemical Co., St. Louis, MO) density centrifugation followed by washing in HBSS. Two separate groups of mice (9 treated and 12 control as described above) were used in these experiments. A total of 100 μCi of ^{99m}Tc were injected i.v. in the tail veins of 9 treated and 12 control mice. After 10 minutes postinjection, tumors and muscle samples were surgically obtained from anesthetized mice. Visible blood vessels were immediately electrocoagulated using a bipolar instrument (Elmed 50/Micro output, Addison, IL) to prevent blood loss from tissues. Blood samples (10-20 μL) were then withdrawn using cardiac puncture and ^{99m}Tc radioactivity was determined using Wallac 1480 γ-counter (Perkin-Elmer, Wellesley, MA) calibrated using ^{99m}Tc standards. Quantitation of hematocrits in individual tissues has been accomplished by using mouse blood standards and assuming negligible immediate changes in hematocrit as a result of i.v. injection of labeled RBC/PGC mixture.

Correction of V_b values. We assumed that longitudinal relaxation time (T1) of the whole blood is affected by RBC volume fraction due to the fact that intravascular contrast agents are distributed almost exclusively in plasma. The blood volume values obtained during the MRI studies were corrected for local differences in RBC content as described in the Supplementary data.

Histology. H&E staining of parallel sections was done using standard protocols. Colon samples were frozen cut after the lumena of the dissected fragments were filled with HistoPrep (Fisher Scientific, Pittsburgh, PA). To assess potential permeability of tumor blood vessels to agents with hydrodynamic diameters similar to that of PGC, several animals were injected with monocrystalline iron oxide nanoparticles (diameter, 20 nm; ref. 34) 20 minutes before euthanasia. Tumors were frozen and 10 μm sections were cut and stained using Perl's stain (Prussian blue reaction) for iron. Staining of endothelial cells in tumors was done by using anti-CD31 antibodies (rat anti-mouse monoclonal, MEC13.3, BD PharMingen, San Diego, CA) labeled with digoxigenin. Binding of antibodies was visualized using anti-digoxigenin F(ab′)$_2$ conjugated with alkaline phosphatase (Roche Diagnostics). Tumor samples for fluorescence microscopy were prepared as in ref. 26 with modifications. Tumor-bearing mice were preinjected with Alexa 488–labeled tomato lectin (50-80 μg/animal in 100 μL of saline) at 15 minutes before euthanasia. Tumors were excised, frozen, and cut into 8 μm sections. Genomic DNA fragmentation in was assessed using terminal deoxyribonucleotidyl transferase–mediated dUTP nick end labeling (TUNEL; ApopTag, Intergen, Purchase, NY) and Cy3-labeled antidigoxigenin F(ab′)$_2$ (Roche Diagnostics). Fluorescence microscopy has been done using Zeiss Axiovert 100 TV (Wetzlar, Germany) fitted with appropriate filter sets (Omega Optical, Brattleboro, VT). Images were acquired using CoolSnapHQ-M CCD (Photometrics, Tucson, AZ) and processed using IP LabSpectrum software (Signal Analytics, Vienna, VA).

Results

Tumor volume, vascular volume, and magnetic resonance imaging of antiangiogenesis. Tumor volumes were monitored using traditional caliper method and MRI. Caliper measurements showed no relative decrease of tumor volume in animals treated with two doses of VEGFR2-TKI versus placebo (Fig. 1*A*). The difference in tumor volumes was evident only in groups 3 and 4 treated for 7 days with placebo or AG013925, respectively (Fig. 1*A*). Parallel MRI measurements of tumor blood volumes (V_b) in animals either treated with placebo or with a KDR inhibitor showed highly statistically significant differences in V_b between experimental and placebo groups ($P < 0.001$; Fig. 1*B*) after two doses of VEGFR2-TKI administered within 1 day (see also Table 1).

MRI of animals with MV522 xenografts revealed small bilateral tumors (Fig. 2*A* and *B*). The tumor blood supply was visible after the injection of PGC-Gd (see Fig. 2*B*, *inset*). On comparative histology, tumors in placebo- and VEGFR-TKI–treated groups

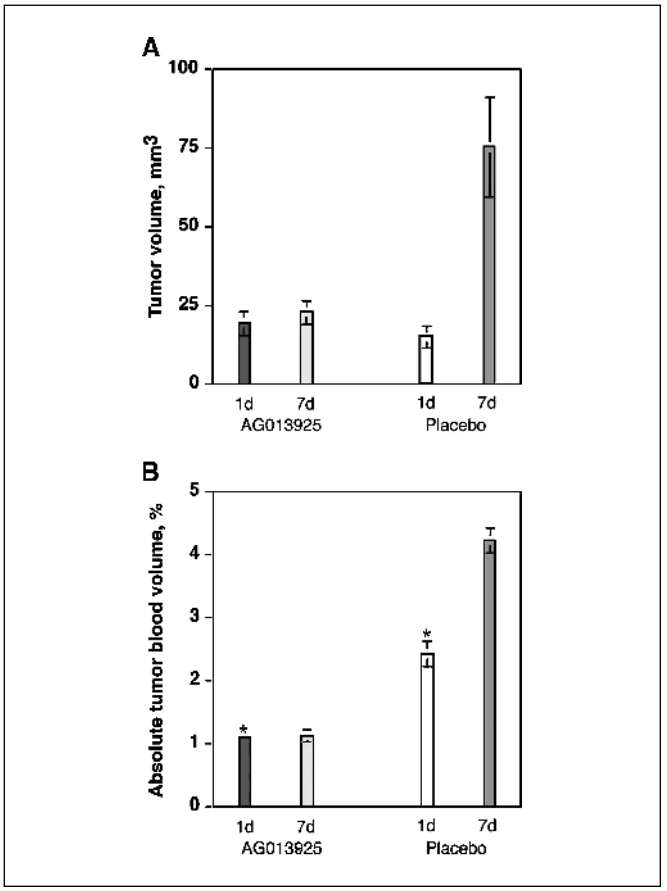

Figure 1. Tumor tissue volume and tumor blood volume as predictors of response to the antiangiogenic treatment. *A,* tumor volumes measured using caliper method in animals either treated with 0.5% CMC (placebo groups 1 and 3) or 25 mg AG013925/kg p.o. b.i.d. (experimental groups 2 and 4). Groups 1 and 2 were treated for 24 hours (2 treatments) whereas groups 3 and 4 were treated for 7 days (14 treatments). There was no statistically significant differences in tissue volumes between experimental and control groups treated for 1 day ($P > 0.2$). *B,* tumor absolute blood volumes (V_b) measured in animal groups shown in *A*. There was a highly significant difference in V_b between experimental and control groups (*, $P < 0.001$). *Columns,* mean; *bars,* SE.

appeared similar, with no extensive necrosis or hemorrhage after two consecutive treatments (Fig. 2*C* and *D*). A control intravascular marker (monocrystalline iron oxide nanoparticles; ref. 35) that could be easily identified in small concentrations in tissues by using iron stain showed no leakage into the interstitium, before or after the treatment (Fig. 2*E*).

High-resolution MRI of colon-implanted orthotopic tumors at 9.4T, using T2-weighted sequences, showed small tumors visible in and around the colon on axial images (Fig. 3*A*, *arrow*). On cross-sectional histology of the colon (Fig. 3*B*), these tumors showed a close shape similarity to *in vivo* magnetic resonance images of the tumors. The T2-weighted images were used for selecting region of interest for T1-weighted signal measurements that were further used for calculating V_b values (see Table 1). The presence and approximate location of these tumors was verified before MRI by using exploratory endoscopy (Fig. 3*C* and *D*). Due to the expression of DsRed2 marker protein, the location of the tumor in colon could be unambiguously verified (Fig. 3*D*). Immunohistology of the tumor invading the colon showed the presence of many small tumors surrounded by vascularized stroma (Fig. 3*E*, *arrows*).

Table 1. Tumor blood volume measured in MV522 xenografts by using MRI and radionuclide determination of hematocrit in tissues of experimental and control animals

	Blood volume (V_b), ectopic tumors, %*		Blood volume (V_b), orthotopic (colon) tumors, %*		Hematocrit (%RBC by volume)	
	Tumor†	Muscle†	Tumor	Muscle	Tumor	Muscle
Placebo 1 d (2 treatments)	2.4 ± 0.1,‡ n = 20	2.6 ± 0.1, n = 14	ND	ND	31 ± 2,§ n = 9	41 ± 1, n = 5
Experiment 1 d (2 treatments)	1.1 ± 0.1,‡ n = 21	3.1 ± 0.1, n = 17	ND	ND	36 ± 1,§ n = 9	40.0 ± 0.5, n = 5
Placebo 7 d (14 treatments)	4.2 ± 0.1,‡ n = 20	3.2 ± 0.1, n = 16	11.9 ± 2.0,§ n = 4	3.9 ± 0.2, n = 4	ND	ND
Experiment 7 d (14 treatments)	1.1 ± 0.1,‡ n = 18	2.8 ± 0.1, n = 23	5.4 ± 1.1,§ n = 4	3.6 ± 0.2, n = 4	ND	ND

NOTE: Animals were used for imaging experiments 1 week after the implantation of MV522 cells as described in Materials and Methods. Placebo-treated mice received 0.5% solution of CMC p.o. b.i.d.; VEGFR2-TKI–treated mice received 25 mg/kg AG013925 suspension in 0.5% CMC p.o. b.i.d. The results are shown as mean ± SE. n, number of MRI slices analyzed per group, or number of animals/group. Statistical significance was determined using Student unpaired t test with Welch's correction, ND, not determined.

*Blood volumes measured under the conditions of the highest accuracy.

†MRI results are corrected for RBC content.

‡Highly statistically significant differences ($P < 0.001$).

§Statistically significant differences ($P < 0.05$).

Using signal intensity analysis of magnetic resonance images, we obtained blood volume measurements at different flip angle values (40°, 60°, and 80°) (Fig. 4*A* and *B*). The high flip angle of 80° used in combination with a very short TE (minimal) and TR = 30 ms provided an accurate measurement of V_b (23). The data obtained with three different flip angles allowed to track the dependence of blood volume on water exchange (i.e., provided information about the change in vascular barrier function as a result of the antiangiogenic treatment). Approximately 1 week after the implantation ectopic tumor, V_b was nearly equivalent to that of the muscle. The mean absolute V_b values determined at 80° were 2.7% and 2.4% of total tissue volume for muscle and tumor, respectively. In the short-term placebo-treated group, the measured ratios of the average V_b determined at 40° and 80° flip angles (R_{flip}) were 1.8 and 1.6 for tumor and muscle, respectively (Fig. 4*A*). After a short-term treatment, V_b decreased for all flip angles (compared with the placebo-treated group, Fig. 4*A*) and R_{flip} values

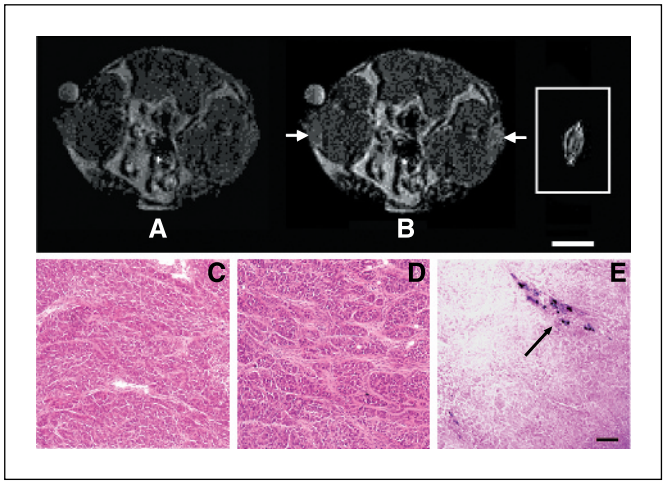

Figure 2. A representative magnetic resonance image of bilaterally implanted ectopic MV522 tumors before the injection of PGC-Gd (*A*) or after the i.v. injection of PGC-Gd (0.1 mL, 50 μmol Gd/kg, *B*). The images (matrix = 256 × 256, slice thickness = 0.7 mm) were obtained at 1.5 T using three-dimensional SPGR pulse sequence; TR/TE = 30/4.1 ms and flip angle of 80°. *Arrows,* tumor location. A fiduciary standard (a tube filled with a 25 μmol/L GdDTPA solution) was placed next to the mouse. *Inset,* a subtraction image showing tumor vasculature contrasted with PGC-Gd. *Bar,* 1 cm. *C,* histology (H&E stain) of MV522 tumor (placebo-treated); *D,* histology (H&E stain) of VEGFR2-TKI (AG01395, 25 mg/kg)–treated tumor; *E,* frozen section of VEGFR2-TKI treated tumor obtained after the i.v. injection of monocrystalline iron oxide nanoparticles (5 mg iron/kg) to delineate perfused blood vessels. *Arrow,* iron-positive Perl's stain. *Bar,* 200 μm.

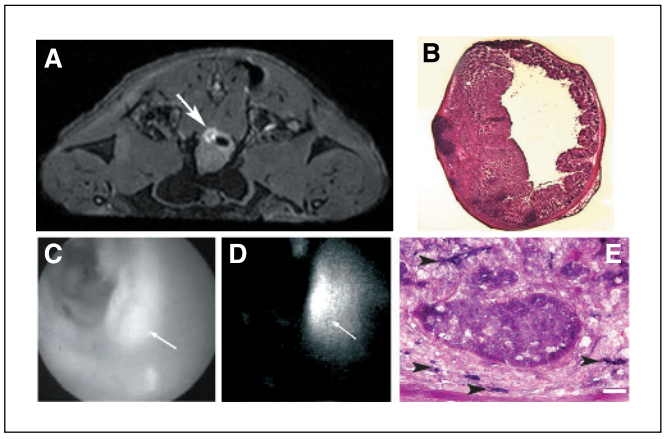

Figure 3. Imaging and histology of orthotopic MV522-DsRed2 colon carcinoma. *A,* MRI of orthotopic MV522-DsRed2 tumor implanted into the colon wall. A T2-weighted image obtained at 9.4T (TR/TE = 3,000/30 ms) is shown. *Arrow,* tumor in the colon. *B,* histology (H&E stain) of MV522-DsRed2 tumor dissected from placebo-treated animal. *C,* visible light image of the tumor obtained by using a microendoscope before treatment. *D,* fluorescence image of the field presented in *C* obtained by exciting fluorescence of DsRed2 using a 300-W Xenon lamp source. *E,* histology of small tumor deposits in the colon wall. *Arrowheads,* CD31-positive microvessels in the stroma. *Bar,* 200 μm.

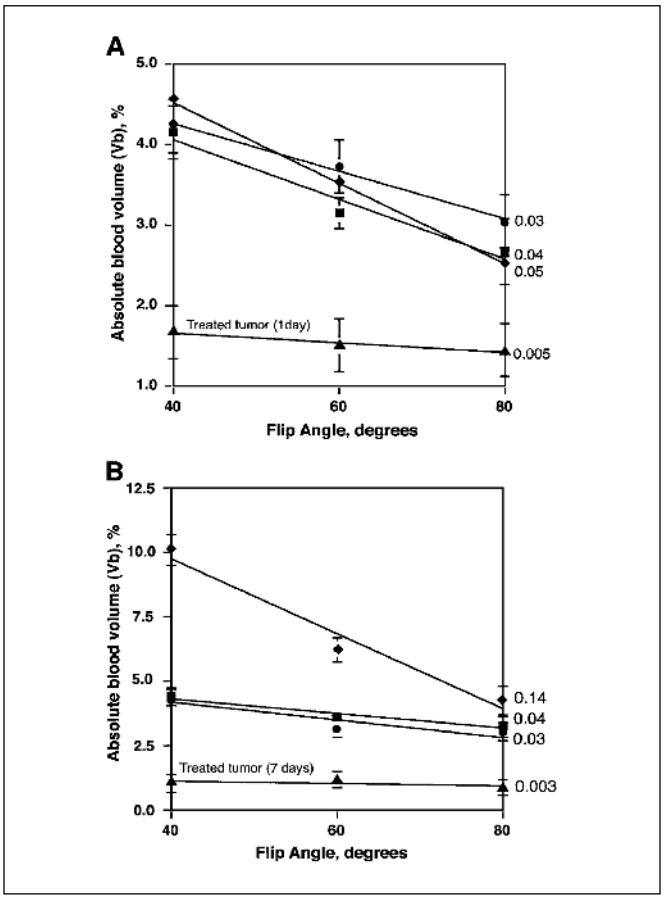

Figure 4. Water exchange rate changes in tumors after the KDR treatment. *A,* absolute blood volume measurements; two doses: control placebo-treated mice (group 1: ♦, tumors; ■, muscle) and AG01395-treated mice (group 2: ▲, tumors; ●, muscle). *B,* absolute blood volume (V_b) measurements; 14 doses: control placebo-treated mice (group 3: ♦, tumors; ■, muscle) and AG01395-treated mice (group 4, ▲, tumors; ●, muscle) using MRI as described in Materials and Methods. Mice were treated p.o. b.i.d. with 25 mg AG013925/kg in 0.5% CMC or 0.5% CMC alone (placebo). A dependence of V_b from flip angle in three-dimensional SPGR pulse sequence is shown. This dependence reflects water exchange rate across the vascular barrier. Negative slopes of the curves are shown at the right. The higher value of the slope corresponds to a faster water exchange. Measurements obtained at a flip angle of 80° resulted in the most accurate V_b value. *Points,* mean; *bars,* SE.

were 1.5 for muscle and 1.1 for tumor. Only in treated tumors there was a substantial suppression of water exchange across the vascular barrier (Fig. 4*A*) because linear approximation of V_b dependence on the flip angle showed a highly attenuated negative slope in comparison with the control tumors. The above linear fitting was valid only at high flip angles (above 40°) used for imaging in this study.

In the placebo-treated group (1 week, group 3), V_b was considerably higher than that of the muscle for flip angles <80° (Fig. 4*B*). The ratio of V_b values obtained at 40° and 80° flip angles was much higher for the tumor than for the muscle (R_{flip} = 2.39 and 1.36, respectively). The high negative slope value (0.14) for placebo-treated tumor (Fig. 4*B*) suggested faster water exchange across vascular barriers in tumor vessels. In contrast, in a group of mice treated with VEGFR2-TKI for 7 days (group 4), the measured tumor V_b was significantly lower than that of the muscle (Fig. 4*B*). The flip angle dependence of V_b in these animals was similar to that of the muscle. The V_b value was nearly constant at all flip angles (negative slope, −0.004), indicating suppression of water exchange (i.e., similar to 1-day treated tumors). In orthotopic tumor–bearing animals treated for 7 days with VEGFR2-TKI, a statistically significant ($P < 0.05$) 2-fold decrease of measured V_b was detected when compared with placebo-treated animals (Table 1). As in the case of ectopic tumor model, no significant changes of V_b in the muscle were observed. Tumor V_b values measured in mouse orthotopic models were much higher than V_b in s.c. ectopic tumors (11.9 ± 2.0% versus 4.2 ± 0.1%).

Radionuclide measurements of RBC fractions in tumors and muscle. The main goal of the radionuclide study was to obtain

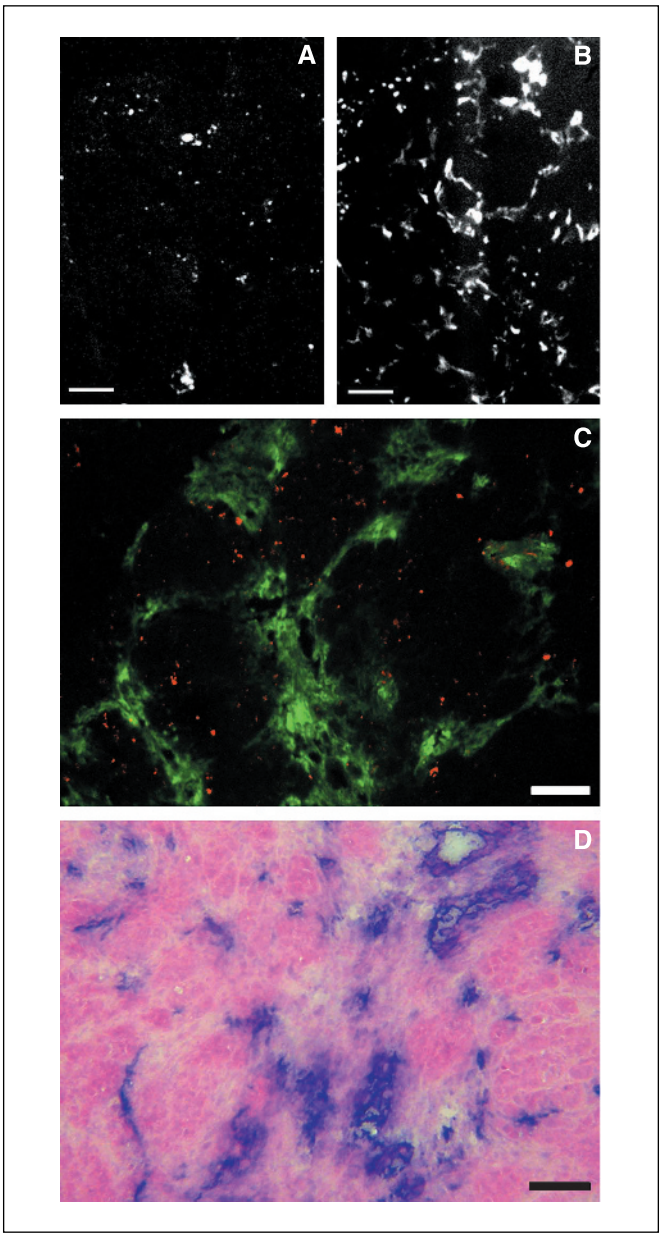

Figure 5. Histology of control tumors (placebo-treated, group 1) obtained from animals injected with Alexa 488–labeled *L. esculentum* lectin. *A,* low-magnification fluorescence microscopy of TUNEL staining of MV522 tumor section; *B,* low-magnification microscopy of fluorescent lectin staining of blood vessels reflecting vascular density. *Bar,* 400 μm. *C,* dual-channel fluorescence microscopy depicting lectin binding (*green*) to vessel-lining cells and TUNEL staining of apoptotic cells; *D,* anti-CD31 staining (microvascular density staining) of blood vessels in control, placebo-treated MV522 tumor followed by H&E staining. *Bar,* 100 μm.

correction factors to account for potential differences in tissue concentration of PGC-Gd (Table 1) by determining RBC content in blood circulating in tumors or normal muscle, respectively. We used ^{99m}Tc-labeled RBC as markers of blood cell volume fraction. Because PGC-Gd is excluded from RBCs, the local concentration of RBC could affect tissue magnetic resonance signal intensity change after the contrast agent injection due to the dilution of PGC-Gd in the plasma by RBCs. By measuring RBC fractions in blood, we accounted for possible measurement error due to the tissue-dependent volume ratio differences between plasma and RBC fractions. As determined by standard hematocrit counting methods, *nu/nu* mice had RBC fraction of 0.4 (40% hematocrit, Table 1). The RBC volume fraction in tumors was only 75% of muscle in the placebo-treated group. However, in the treated group of animals, the tumor blood RBC fraction was nearly equivalent to that of the muscle. We found that the difference between corrected and experimental V_b values was negligibly small in treated animals. In placebo-treated mice, experimental V_b values for tumors were significantly different from corrected V_b because of the reduced RBC fraction in tumoral circulation.

Histology. To determine whether the measured changes in blood volume were reflecting changes in tumor vascular density and vascular architecture, we did histology of tumors. After *in vivo* injection of fucose-specific fluorescent-labeled lectin (Figs. 5–7), we observed bright fluorescence of vascular wall. In parallel, TUNEL staining of histology sections was done. The numbers of fluorescent (apoptotic) nuclei were relatively low in MV522 placebo-treated tumors (7 ± 3 cells/mm^2 tumor section area, Fig. 5*A*). The density of perfused microvessels in these tumors was very high (69 ± 20 lectin-positive vessels/mm^2 tumor section area, Fig. 5*B*). Similar vascular density counts were obtained by using anti-CD31 anti-bodies (80 ± 22 vessels/mm^2). Blood vessels appeared dilated and highly positive for fluorescent lectin (Fig. 5*C*). The difference between microvascular density counts obtained using *in vivo* fluorescent lectin labeling and anti-CD31 staining (Fig. 5*D*) did not exceed 16%. If compared with the placebo group, VEGFR2-TKI treatment resulted in a 7-fold increase in the number of TUNEL-positive cells (48 ± 6 cells/mm^2, Fig. 6*A*). This increase paralleled an average of a 3-fold decrease of the blood vessel density (20 ± 10 vessel/mm^2, Fig. 6*B* and *E*). Normal muscle adjacent to the tumor showed intact vascularity (Fig. 6*D*). However, blood vessels at the border of the tumor and muscle contained TUNEL-positive cells lining lectin-positive vessels (Fig. 6*D*). Endothelial cell death was also observed in some small-diameter vessels on the periphery of tumors that were stained positively for DNA fragmentation and lectin (Fig. 7*A* and *B*, *arrows*). Histology of tumors after a 7-day treatment revealed regions of apoptosis. The areas of tumor cell death seemed to be more extensive than that of 2-day treated tumors. Apoptosis-free areas of tumors were sustained by a few small-diameter vessels that were positive for lectin and anti-CD31 antibody (Fig. 7*C*).

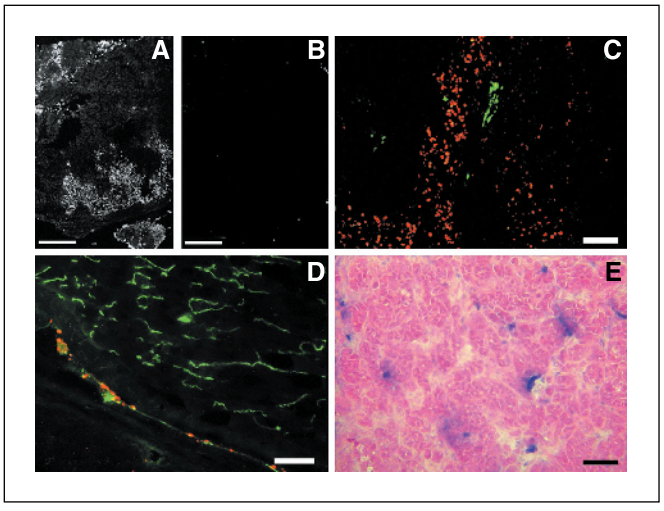

Figure 6. Histology of MV522 tumors treated with antiangiogenic VEGFR2-TKI AG01395, 25 mg/kg p.o. (group 2) obtained from animals injected with Alexa 488–labeled *L. esculentum* lectin (*A-D*). Images were obtained using fluorescence microscopy of tumors. *A,* low-magnification microscopy of TUNEL staining of tumor section. *B,* low-magnification microscopy of fluorescent lectin staining of blood vessels reflecting vascular density. *A* and *B*, bar = 400 μm. *C,* dual-channel fluorescence microscopy depicting lectin binding (*green*) to vessel-lining cells and TUNEL staining of apoptotic cells. *D,* fluorescent image of the tumor/muscle interface showing a blood vessel with TUNEL-positive cells. Note the high density of vascularization of the muscle and nearly absent vascularization of the treated tumor. *E,* anti-CD31 staining (microvascular density staining) of blood vessels in VEGFR2-TKI–treated MV522 tumor followed by H&E staining. Animals were treated with two doses at 25 mg/kg with 12-hour interval in between the treatments. *C* to *E*, bar = 100 μm.

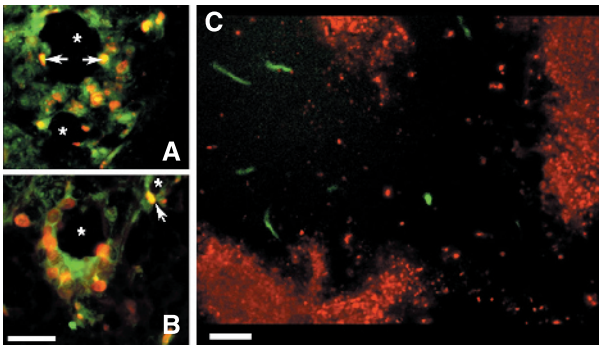

Figure 7. TUNEL analysis of MV522 tumors. *A* and *B,* representative micrographs of tumor peripheral vessels showing apoptosis of vessel-lining cells. *Arrows,* cells morphologically similar to endothelial cells stained with Alexa 488–labeled *L. esculentum* lectin. *, vascular lumena. *Bar,* 50 μm. *C,* fluorescent image depicting a section of 7-day treated MV522 tumor showing areas of cell death (*red*) and surviving blood vessels (*green*). *Bar,* 100 μm.

Discussion

Noninvasive imaging of blood volume changes in tumors as well as tumoral vascular permeability measurements enable the assessment of antiangiogenic (or angiostatic) therapies in live animals (reviewed in ref. 16). It has been suggested that tumor blood volume monitoring in preclinical and clinical research could be valuable for detecting early changes of tumor homeostasis mediated by antiangiogenesis drugs and in predicting the response of cancer to a specific type of drug treatment as has been shown in the case of combretastatin (36) or dexamethasone (37).

We report here noninvasive imaging analysis of the antiangiogenic effects of a VEGFR2-TKI in ectopic as well as orthotopic MV522 xenograft tumor models. We anticipated that the inhibitor was capable of inducing dramatic changes in tumor blood supply at the very early phase of the treatment. Our decision to explore blood volume changes rather than vascular permeability was due to the anticipated strong antitumor effects of VEGFR2-TKI. Vascular collapse as a result of endothelial cell death or tumor vessel regression (10) drastically decreases the overall vascular area in the tumor, especially in the tumor periphery (38). The above

effect would make it impossible to compare the relative changes of vascular permeability in the tumor ("permeability-surface area product"; refs. 39–41) before and after the treatment. Therefore, we imaged tumor blood volume using MRI enhanced with a long-circulating, biocompatible, and nontoxic paramagnetic T1 contrast agent (PGC; ref. 27). This contrast agent is known to selectively decrease relaxation times of water protons in the vascular compartment without any initial leakage from blood vessels due to a large hydrodynamic diameter corresponding to a globular protein of 1,500 kDa (42).

The analysis of MRI results was valid under the following assumptions: (*a*) the movement of protons between extracellular and cellular compartments in the blood was considered rapid allowing to treat RBC and plasma as one vascular space (two-compartment Hazelwood model; ref. 23); (*b*) the kinetics of extravascular-intravascular water exchange was slower or comparable to the time required to obtain an image within the selected tissue volume; (*c*) there was no appreciable leakage of the paramagnetic probe (PGC-Gd) into the interstitium of tumors during the imaging experiment (23, 25, 42). The latter assumption was confirmed by using a model nanoparticle agent (see Fig. 2). By comparing initial tumor volume data with the results of V_b measurements, we observed that unlike tumor tissue volume (Fig. 1*A*), tumor blood volume (Fig. 1*B*) responded dramatically to VEGFR2-TKI showing a decrease at the very early phase of treatment (i.e., after two doses of the antiangiogenic drug). Furthermore, the analysis of vascular water exchange rates in tissues of control and treated animals, by examining the measurement dependency of V_b on flip angle (33), suggested a tissue-dependent disparity in water exchange rates across the vascular membrane in the muscle and the nearby tumor. Both V_b and water exchange rate were maintained at the low levels over the course of the treatments, suggesting the effective suppression of angiogenesis by VEGFR2-TKI (see Fig. 4).

The exclusion of paramagnetic PGC-Gd from RBC in local circulation could potentially introduce tissue-dependent measurement inaccuracies due to local differences in blood composition in normal and tumor blood vessels. The radioisotope-labeled RBC study showed an increase of RBC fraction in the remaining blood supply of the tumors after the treatment, whereas RBC fraction in the muscle remained constant (Table 1). The low tumoral RBC fraction in placebo-treated mice was probably caused by abnormal architecture of the neovasculature. The increase of RBC content in blood supply of treated tumors suggests that after the VEGFR2-TKI treatment, tumor neovasculature undergoes partial "normalization," a general effect observed by intravital microscopy after various antiangiogenic treatments (43, 44). Alternatively, the above results may indicate that there is a fraction of co-opted tumor vessels that exhibit a very low degree of endothelial proliferation (45). These vessels could be spared from regression as a result of antiangiogenic treatment or VEGF withdrawal (46). In the case of VEGFR2-TKI treatment, the latter scenario seems probable. It should be noted that in orthotopic MV522-DsRed2 tumors, VEGFR2-TKI resulted in a lesser relative V_b decrease if compared with their ectopic counterparts. This could be explained by the tumor-mediated co-option of preexisting vessels (47) as opposed to *de novo* angiogenesis and, consequently, a lack of susceptibility of these vessels to treatments that affect predominantly proliferating endothelial cells. Histology of treated and control tumors revealed that surviving vessels were present in treated tumors in very small numbers (Fig. 6). The observed drastic decrease of blood supply (compare Figs. 5 and 6) suggested that rapid and extensive apoptosis of tumor cells could be explained either by permanent or transient interruption of vascular perfusion resulting from VEGFR2-TKI treatment. The treatment resulted in endothelial apoptosis. Although in majority of histology sections endothelial apoptosis could not be differentiated from tumor cell death, some of the remaining vessels on tumor periphery showed an evidence of vessel-lining cell apoptosis, which seems to correlate with antiangiogenic treatment (Figs. 6*D* and 7*A-B*). Whereas some of the TUNEL-positive cells resemble endothelial cells (Fig. 7*A* and *B*), VEGFR2-TKI could cause death in cells besides endothelial cells (e.g., pericytes or other mural cells as well as stromal fibroblasts expressing PDGF receptor β; ref. 5). The prolonged treatment of tumor-bearing animals with VEGFR2-TKI suggested that some of the remaining tumor blood vessels were perfused and provided survival of the adjacent tumor cells (Fig. 7*C*) but did not allow tumor expansion (Fig. 1).

In conclusion, quantitative MRI enabled noninvasive monitoring of the longitudinal changes in tumor blood volume that responded very early to antiangiogenic therapy with VEGFR2-TKI. The decrease of V_b was tumor specific and concomitant to massive tumor cell/endothelial apoptosis, decrease of vascular density, and increase of RBC content in the residual tumor blood supply. The MRI-assisted analysis of V_b could be an important adjunct in evaluating antiangiogenic therapies in preclinical research and clinical practice.

Acknowledgments

Received 8/21/2003; revised 7/12/2005; accepted 8/9/2005.

Grant support: NIH grants 1P50CA86355-01 (Project 2) and 5RO1 CA74424-01 (A. Bogdanov, Jr.), German National Academy Foundation (Studienstiftung; W. Reichardt); and NIH Research Supplement for Underrepresented Minorities (D. Torres).

The costs of publication of this article were defrayed in part by the payment of page charges. This article must therefore be hereby marked *advertisement* in accordance with 18 U.S.C. Section 1734 solely to indicate this fact.

We thank Dr. David Shalinsky (Pfizer Global Research and Development) for useful discussions. We also thank Dr. Pallab Banerjee (University of Massachusetts Medical School, Worcester, MA) for providing stable MV522-DsRed2 cell lines.

References

1. Iqbal S, Lenz HJ. Angiogenesis inhibitors in the treatment of colorectal cancer. Semin Oncol 2004;31: 10–6.
2. Vajkoczy P, Menger MD, Vollmar B, et al. Inhibition of tumor growth, angiogenesis, and microcirculation by the novel Flk-1 inhibitor SU5416 as assessed by intravital multi-fluorescence videomicroscopy. Neoplasia 1999;1: 31–41.
3. Laird AD, Vajkoczy P, Shawver LK, et al. SU6668 is a potent antiangiogenic and antitumor agent that induces regression of established tumors. Cancer Res 2000;60: 4152–60.
4. Shaheen RM, Davis DW, Liu W, et al. Antiangiogenic therapy targeting the tyrosine kinase receptor for vascular endothelial growth factor receptor inhibits the growth of colon cancer liver metastasis and induces tumor and endothelial cell apoptosis. Cancer Res 1999; 59:5412–6.
5. Mendel D, Laird A, Xin X, et al. *In vivo* antitumor activity of SU11248, a novel tyrosine kinase inhibitor targeting vascular endothelial growth factor and platelet-derived growth factor receptors: determination of a pharmacokinetic/pharmacodynamic relationship. Clin Cancer Res 2003;9:327–37.
6. Drevs J, Hofmann I, Hugenschmidt H, et al. Effects of PTK787/ZK 222584, a specific inhibitor of vascular endothelial growth factor receptor tyrosine kinases, on primary tumor, metastasis, vessel density, and blood flow in a murine renal cell carcinoma model. Cancer Res 2000;60:4819–24.
7. Drevs J, Muller-Driver R, Wittig C, et al. PTK787/ZK 222584, a specific vascular endothelial growth factor-receptor tyrosine kinase inhibitor, affects the anatomy of the tumor vascular bed and the functional vascular

properties as detected by dynamic enhanced magnetic resonance imaging. Cancer Res 2002;62:4015–22.
8. Fabbro D, Buchdunger E, Wood J, et al. Inhibitors of protein kinases: CGP 41251, a protein kinase inhibitor with potential as an anticancer agent. [Review] [52 refs]. Pharmacol Ther 1999;82:293–301.
9. Fabbro D, Ruetz S, Bodis S, et al. PKC412—a protein kinase inhibitor with a broad therapeutic potential. Anti-Cancer Drug Design 2000;15:17–28.
10. Tetsuichiro I, Mancuso M, Hashizume H, et al. Inhibition of vascular endothelial growth factor (VEGF) signaling in cancer causes loss of endothelial fenestrations, regression of tumor vessels, and appearance of basement membrane ghosts. Am J Pathol 2004;165: 35–52.
11. Turetschek K, Preda A, Floyd E, et al. MRI monitoring of tumor response to a novel VEGF tyrosine kinase inhibitor in an experimental breast cancer model. Acad Radiol 2002;9:S519–20.
12. Bhujwalla ZM, Artemov D, Natarajan K, Solaiyappan M, Kollars P, Kristjansen PE. Reduction of vascular and permeable regions in solid tumors detected by macromolecular contrast magnetic resonance imaging after treatment with antiangiogenic agent TNP-470. Clin Cancer Res 2003;9:355–62.
13. Neeman M, Provenzale J, Dewhirst M. Magnetic resonance imaging applications in the evaluation of tumor angiogenesis. Semin Radiat Oncol 2001;11:70–82.
14. Neeman M. Functional and molecular MR imaging of angiogenesis: seeing the target, seeing it work. J Cell Biochem 2002;39:11–7.
15. Choyke PL, Dwyer AJ, Knopp MV. Functional tumor imaging with dynamic contrast-enhanced magnetic resonance imaging. J Magn Reson Imaging 2003;17: 509–20.
16. McDonald DM, Choyke PL. Imaging of angiogenesis: from microscope to clinic. Nat Med 2003;9:713–25.
17. Brasch R, Pham C, Shames D, et al. Assessing tumor angiogenesis using macromolecular MR imaging contrast media. J Magn Reson Imaging 1997;7:68–74.
18. Lin W, Paczynski RP, Kuppusamy K, Hsu CY, Haacke EM. Quantitative measurements of regional cerebral blood volume using MRI in rats: effects of arterial carbon dioxide tension and mannitol. Magn Reson Med 1997;38:420–8.
19. Su MY, Jao JC, Nalcioglu O. Measurement of vascular volume fraction and blood-tissue permeability constants with a pharmacokinetic model: studies in rat muscle tumors with dynamic Gd-DTPA enhanced MRI. Magn Reson Med 1994;32:714–24.
20. Dennie J, Mandeville J, Boxerman J, Packard S, Rosen B, Weisskoff R. NMR imaging of changes in vascular morphology due to tumor angiogenesis. Magn Reson Med 1998;40:793–9.
21. Mandeville JB, Marota JJ, Kosofsky BE, et al. Dynamic functional imaging of relative cerebral blood volume during rat forepaw stimulation. Magn Reson Med 1998; 39:615–24.
22. Boxerman JL, Hamberg LM, Rosen BR, Weisskoff RM. MR contrast due to intravascular magnetic susceptibility perturbations. Magn Reson Med 1995;34:555–66.
23. Donahue KM, Weisskoff RM, Chesler DA, et al. Improving MR quantification of regional blood volume with intravascular T1 contrast agents: accuracy, precision, and water exchange. Magn Reson Med 1996;36: 858–67.
24. Meyer KL, Joseph PM, Mukherji B, Livolsi VA, Lin R. Measurement of vascular volume in experimental rat tumors by 19-F magnetic resonance imaging. Invest Radiol 1993;28:710–9.
25. Weissleder R, Cheng HC, Marecos E, Kwong K, Bogdanov A, Jr. Non-invasive *in vivo* mapping of tumour vascular and interstitial volume fractions. Eur J Cancer 1998;34:1448–54.
26. Petrovsky A, Schellenberger E, Josephson L, Weissleder R, Bogdanov A, Jr. Near-infrared fluorescent imaging of tumor apoptosis. Cancer Res 2003;63: 1936–42.
27. Bogdanov A, Jr., Weissleder R, Frank HW, et al. A new macromolecule as a contrast agent for MR angiography: preparation, properties, and animal studies. Radiology 1993;187:701–6.
28. Bogdanov A, Jr., Marecos E, Cheng HC, et al. Treatment of experimental brain tumors with thrombospondin-1 derived peptides: an *in vivo* imaging study. Neoplasia 1999;1:438–45.
29. Shalinsky DR, Brekken J, Zou H, et al. Marked antiangiogenic and antitumor efficacy of AG3340 in chemoresistant human non-small cell lung cancer tumors: single agent and combination chemotherapy studies. Clin Cancer Res 1999;5:1905–17.
30. Shalinsky DR, Brekken J, Zou H, et al. Broad antitumor and antiangiogenic activities of AG3340, a potent and selective MMP inhibitor undergoing advanced oncology clinical trials. Ann N Y Acad Sci 1999;878:236–70.
31. Funovics MA, Weissleder R, Mahmood U. Imaging enzyme activity and gene expression *in vivo* through a 2.7F catheter. Radiology 2004;231:659–66.
32. Cox R. AFNI: Software for analysis and visualization of functional magnetic resonance neuroimages. Comput Biomed Res 1996;29:162–73.
33. Kim Y, Rebro K, Schmainda K. Water exchange and inflow affect the accuracy of T1-GRE blood volume measurements: implication for the evaluation of tumor angiogenesis. Magn Reson Med 2002;47:1110–20.
34. Shen T, Weissleder R, Papisov M, Bogdanov A, Jr., Brady TJ. Monocrystalline iron oxide nanocompounds (MION): physicochemical properties. Magn Reson Med 1993;29:599–604.
35. Bremer C, Mustafa M, Bogdanov A, Jr., Ntziachristos V, Petrovsky A, Weissleder R. Steady-state blood volume measurements in experimental tumors with different angiogenic burdens a study in mice. Radiology 2003;226: 214–20.
36. Anderson HL, Yap JT, Miller MP, Robbins A, Jones T, Price PM. Assessment of pharmacodynamic vascular response in a phase I trial of combretastatin A4 phosphate. J Clin Oncol 2003;21:2823–30.
37. Badruddoja MA, Krouwer HG, Rad SD, Rebro KJ, Pathak PA, Schmainda KM. Antiangiogenic effects of dexamethasone in 9L gliosarcoma assessed by MRI cerebral blood volume maps. Neuro-oncol 2003;5: 235–43.
38. Vajkoczy P, Thurnher A, Hirth KP, et al. Measuring VEGF-Flk-1 activity and consequences of VEGF-Flk-1 targeting *in vivo* using intravital microscopy: clinical applications. Oncologist 2000;5 Suppl 1:16–9.
39. Schwickert HC, Stiskal M, Roberts TP, et al. Contrast-enhanced MR imaging assessment of tumor capillary permeability: effect of irradiation on delivery of chemotherapy. Radiology 1996;198:893–8.
40. Furman-Haran E, Margalit R, Grobgeld D, Degani H. Dynamic contrast-enhanced magnetic resonance imaging reveals stress-induced angiogenesis in MCF7 human breast tumors. Proc Natl Acad Sci U S A 1996; 93:6247–51.
41. Demsar F, Roberts TP, Schwickert HC, et al. A MRI spatial mapping technique for microvascular permeability and tissue blood volume based on macromolecular contrast agent distribution. Magn Reson Med 1997;37:236–42.
42. Lewin M, Bredow S, Sergeyev N, Marecos E, Bogdanov A, Jr., Weissleder R. *In vivo* assessment of vascular endothelial growth factor-induced angiogenesis. Int J Cancer 1999;83:798–802.
43. Jain RK. Normalizing tumor vasculature with anti-angiogenic therapy: a new paradigm for combination therapy. Nat Med 2001;7:987–9.
44. Izumi Y, Xu L, di Tomaso E, Fukumura D, Jain RK. Tumour biology: herceptin acts as an anti-angiogenic cocktail. Nature 2002;416:279–80.
45. Bergers G, Benjamin L. Tumorigenesis and the angiogenic switch. Nat Rev Cancer 2003;3:401–10.
46. Abramovitch R, Dafni H, Smouha E, Benjamin L, Neeman M. *In vivo* prediction of vascular susceptibility to vascular susceptibility endothelial growth factor withdrawal: magnetic resonance imaging of C6 rat glioma in nude mice. Cancer Res 1999;59:5012–6.
47. Lu W, Schroit A. Vascularization of melanoma by mobilization and remodeling of preeexisting latent vessels to patency. Cancer Res 2005;65:913–8.